CONTROLLING HYDROGEN EMBRITTLEMENT IN ULTRA-HIGH STRENGTH STEELS

John R. Scully, Hakan Dogan, Daoming Li, and Richard P. Gangloff
Center for Electrochemical Science and Engineering
Department of Materials Science and Engineering
University of Virginia
Charlottesville, VA 22904-4745
USA

ABSTRACT

A Fe-13Co-11Ni-3Cr-1Mo-0.2C steel alloy, processed for ultra-high strength and fracture toughness, exhibits three distinct hydrogen trap states in a complex precipitation hardened martensitic microstructure and is susceptible to severe hydrogen embrittlement (HE) at threshold stress intensity levels as low as 20 MPa√m. The causes of HE susceptibility include very high crack-tip tensile stresses and a reservoir of diffusible hydrogen that is trapped reversibly with a binding energy, E_b, of 11.5±0.5 kJ/mol at $(Fe,Cr,Mo)_2C$ precipitates. This reversibly trapped hydrogen repartitions to interstitial sites proximate to the highly stressed crack tip and, subsequently, may retrap at martensitic lath interfaces to produce substantial local hydrogen concentrations and transgranular embrittlement. These results are pertinent to the control of HE in this modern ultra-high strength steel with a cadmium-plated coating and co-deposited hydrogen (H). Thermal Desorption Spectroscopy demonstrates that 190°C baking removes the detrimental hydrogen associated with $(Fe,Cr,Mo)_2C$ traps in both precharged but unplated steel as well as in thin porous, cadmium-plated steel. Restoration of a high fracture toughness and a ductile fracture mode correlates directly with the removal of hydrogen from $(Fe,Cr,Mo)_2C$ traps as well as other low energy trap states. However, the internal H concentration at such traps is at first intensified upon baking of cadmium-plated steel. Later H egress is retarded by the slow H diffusivity in steel and the barrier action of the cadmium plating. Hydrogen trapped at higher trap binding energy sites is not removed by 190°C baking, but cannot redistribute to the crack tip fracture process zone and does not participate in subcritical hydrogen cracking. Strategies for controlling hydrogen embrittlement are proposed based on the information generated.

Keywords: ultra-high strength steel, hydrogen embrittlement, hydrogen trapping, thermal baking, cadmium plating.

INTRODUCTION

Ultrahigh-strength steel (UHSS) enables high performance aerospace structures that require high tensile strength and fracture toughness.[1,2] A secondary hardening UHSS, Fe-13Co-11Ni-3Cr-1Mo-0.2C (AerMet® 100,[(1)]), was developed to provide plane strain fracture toughness (K_{IC}) in excess of 120 MPa√m, doubling that of

[(1)] AerMet 100 is a trademark of Carpenter Technology Corp., Reading, PA 19612-4662

older steels such as AISI 4340 and 300M, each at constant yield strength (σ_{YS}) of 1750 MPa.[3,4] This strength is produced by a homogeneous distribution of nanoscale coherent $(Fe,Cr,Mo)_2C$ alloy carbides in Fe-Ni martensite laths that are highly dislocated due to Co retardation of recovery.[5,6] The high K_{IC} is achieved by advanced melting to minimize S + P and inclusion contents, austenitization to control undissolved carbides and grain size, and aging to optimize austenite precipitates along martensite lath interfaces.[2,4,7,8]

Ultra-high strength steels are susceptible to severe internal hydrogen embrittlement (IHE) as well as hydrogen environment embrittlement (HEE), and Fe-13Co-11Ni-3Cr-1Mo-0.2C steel is no exception.[9] Several studies demonstrated subcritical HEE at apparent threshold stress intensity (K_{TH}) levels as low as 20-30 MPa√m when the microstructure, optimized for high K_{IC} (~ 130 MPa√m), was stressed in neutral chloride near the free corrosion potential.[10-12] UHSS is often electroplated for corrosion resistance, introducing the potential for IHE.[13,14] Thomas and coworkers demonstrated that optimally aged Fe-13Co-11Ni-3Cr-1Mo-0.2C steel is susceptible to severe IHE at K_{TH} levels as low as 20 MPa√m and produced by diffusible H contents as low as 1 part-per-million by weight (wppm).[15] Both IHE and HEE in Fe-13Co-11Ni-3Cr-1Mo-0.2C steel are predominantly transgranular (TG), associated with cracking of interfaces in the martensitic microstructure.[10-12,15-17] The TG H-cracking mode is traced to the low concentration of metalloid impurities segregated to austenite grain boundaries, to minimize intergranular cracking, coupled with substantial H accumulation by trapping at transgranular sites in the crack tip process zone.[9,15]

Cadmium electroplating produces a protective coating on steel surfaces that improves corrosion resistance, but atomic hydrogen (H) can be co-deposited during plating and may enter the steel substrate.[13,14] A post-plating baking process is frequently required to remove this residual H,[13,14,18-20] however, effectiveness has been questioned for UHSS such as AISI 4340.[13,14,21] A coating can further complicate H egress/desorption during baking exposure by acting as a diffusion barrier and H source. For electroplated Cd, H is co-deposited in both the Cd coating and steel substrate.[13,14,21] The H concentration in the steel increases during the early stage of baking with the electroplated Cd layer serving as a H source, since H solubility in Cd is higher than that in Fe.[13,14,21] The Cd layer also acts as a diffusion barrier during baking, due to a much slower H diffusivity in Cd than in steel.[21] Hence, considerable-diffusible H may remain in a baked steel, even after heating for 100 h.[13] The 1-5 wppm level of residual-dissolved H, typical of Cd plating and subsequent baking, embrittles high strength AISI 4340 steel.[22] Similar problems were reported for Cd-plated steel fasteners.[23]

The influences of H trapping on IHE and HEE are important and complex.[24-27] The amount of residual trapped hydrogen depends on the time-temperature conditions during baking. The chance that trapped hydrogen redistributes to the crack tip or resides along a connected crack path depends on the details of trapping, baking, microstructure, and local stress. Therefore, the outcome of baking is complicated. A typical example was evidenced for a high carbon steel where baking at 200°C dramatically increased embrittlement susceptibility.[20] Reversible trap sites with low binding energy provide a reservoir of mobile H that diffuses to areas of lower H chemical potential, such as the dilated region associated with triaxial tensile stress ahead of a crack tip. Such traps exacerbate IHE, as illustrated by decreasing threshold stress intensity with increasing diffusible H concentration reported for AISI 4340-type steels,[28-30] as well as Fe-13Co-11Ni-3Cr-1Mo-0.2C steel.[15] In contrast, a homogeneous distribution of irreversible or strong-reversible traps, that do not constitute a connected path of fracture initiation sites and resist H repartitioning to the hydrostatic tensile stress field of a crack tip, may not play a role in IHE or may shield the material from brittle H cracking.[31-33]

There is limited information on which trap states govern IHE compared to those that release H when baked at specified temperatures. Previous work demonstrated that weak or reversible trap sites provide a reservoir of mobile H that is capable of diffusing to the crack tip process zone and exacerbating IHE.[29-31] There may be considerable residual H in higher energy (reversible) trap sites after conventional baking treatment.[8] Whether such H repartitions to the hydrostatically stressed region ahead of a crack tip and facilitates embrittlement depends on the energetics of trapping at microstructural features compared to the energetics of stress field occlusion. For a microstructure containing plentiful trap sites, it is necessary to consider the effectiveness of baking in removing hydrogen from various trap states.[34,35] It is important to compare the trap binding energies of states that liberate hydrogen at conventional baking temperatures to the trap states that are important in IHE.

In a recent study on H trapping states in Fe-13Co-11Ni-3Cr-1Mo-0.2C steel, various H traps with different binding energies were identified and assigned to fine-scale microstructural features.[36] A H desorption shoulder at low temperatures (<100°C) was likely associated with lattice H, whereas at least three distinct desorption peaks were ascribed to different reversible and irreversible trap states. The first and dominant trap state is attributed to predominant H trapping at $(Fe,Cr,Mo)_2C$ precipitates (peak 1b), in addition to possible alloying solute and martensitic substructure (peak 1a). This trap state possesses a very high H trap occupancy (N_r/N_L of 0.03-0.07, where N_r is the number of reversible trap sites per unit volume and N_L is the number of ordinary interstitial sites available for H in the perfect lattice). Energy analysis established H repartition from this trap state to the crack tip in UHSS under the influence of high-hydrostatic stress.[36] In contrast the second and third trap states (peaks 2 and 3) are associated with H trapping at strong trap sites such as martensite interfaces, austenite grain boundaries, mixed dislocation cores, and undissolved metal carbides. It seems unlikely that H repartitions to the crack tip from these high-energy trap states for a practically attainable hydrostatic stress.[36] Information on release of hydrogen and residual hydrogen at trap states capable of supplying hydrogen to the crack tip is, therefore, necessary to control hydrogen embrittlement either through baking practice or microstructural optimization.

The objective of this research is to establish the effect of baking on H detrapping and egress from electroplated UHSS. Specifically, the influence of thermal baking on H desorption is characterized for electrochemically charged bare, thin and thick cadmium plated Fe-13Co-11Ni-3Cr-1Mo-0.2C steel. The focus is on H egress as a function of H trap state, as established systematically by varying baking time at fixed baking temperature. The baking temperature for embrittlement relief is specified as 190-220°C for steels having tensile strength of 1000 MPa and higher (Table 1);[19] thus, 190°C was selected for study. The amount of H desorbed during baking from each trap state was quantified by both electrochemical extraction and thermal desorption methods, and correlated with restoration of fracture toughness. The results of these experiments provide basic understanding that better enables control of IHE in Fe-13Co-11Ni-3Cr-1Mo-0.2C steel.

EXPERIMENTAL PROCEDURES

Material

The material selected for the present investigation was Fe-13Co-11Ni-3Cr-1Mo-0.2C steel. This alloy, of composition shown in Table 2, was received as annealed bar (15.2 cm in diameter and 30.5 cm long). To achieve an optimal strength and toughness combination, specimens were vacuum heat-treated as follows: solution treat at 885°C for 1 h, air cool to room temperature in 2 h, chill at -73°C for 1 h, and temper at 482°C for 5 h.[37,38] Major mechanical properties resulting from this treatment are given in Table 3.[15] While the microstructure is detailed elsewhere,[5-7] the main features relevant to this study are: (1) less than 0.1 μm diameter incoherent carbides (i.e., $(MoCr)_7C_3$, $(FeCr)_XC_Y$, TiC, (TiCrMo)C) that provide grain refinement, (2) prior austenite grain boundaries, (3) martensite laths on the order of 0.15 μm thick, both twinned and un-twinned, with interfaces that are high-angle and arrayed in packets, (4) dislocations in martensite and not recovered at this tempering temperature, (5) finely distributed, partly coherent M_2C (where M = 75 at.% Cr, 13 Fe and 12 Mo) in martensite, averaging 2 nm diameter x 8 nm length, (6) Cr and/or Mo dissolved in coherent clusters in martensite, (7) Co dissolved in martensite, perhaps with short range order, (8) precipitated austenite, and (9) Ni dissolved in austenite. Retained austenite is negligible due to refrigeration.[5] Precipitated austenite is present as a thin layer (~ 3 nm) at martensite lath interfaces based on electron microscopy, but the volume fraction from X-ray diffraction measurements is uncertain, ranging from an average volume pct of 0.8 [3] to 4 [6] for the 482°C temper.

Electrochemical hydrogen charging

Planar steel coupons were ground to 600-grit surface finish, degreased with methanol and H charged in saturated $Ca(OH)_2$ (pH ~ 12.1), prepared with pre-electrolyzed 18.2 MΩ deionized water. Hydrogen charging was performed at various constant H overpotentials ($\eta_{chg} = E_{Applied} - E_{RH^+/H}$) under potentiostatic control at either 23°C or 60°C. The calculated reversible H oxidation/reduction potential, $E_{RH^+/H}$, in this solution was –1.330 V (*vs*

Hg/Hg_2SO_4). Charging time necessary to develop a uniform hydrogen concentration was calculated from a saturation curve given by a solution for Fick's second law for one-dimensional diffusion in a planar sheet with conservative estimates of the trap-affected apparent hydrogen diffusivity (D_H) of 8 x 10^{-9} cm^2/s at 23°C and 3 x 10^{-8} cm^2/s at 60°C.[39] As-charged specimens were stored in liquid nitrogen for testing as needed.

Cadmium plating, baking and stripping

Cadmium plating was according to the QQ-P-416F standard as Type I (As-Plated) CLASS 3.[40] Two different batches were plated, with Cd thickness of 18 μm (Batch I) and 10 μm (Batch II).[41] Prior to plating, specimens were ground to 600-grit surface finish, cleaned with methanol, rinsed with distilled water, and air-dried. Cadmium plating parameters were: sodium cyanide (NaCN) bath with a cyanide concentration of 128.5 g/L and pH of 11.7, cathodic current density of 0.15 to 0.20 A/cm^2 and cadmium metal concentration of 31 g/L. Plating was conducted at ambient temperature for 30 minutes. Following plating, specimens were rinsed with water, dried and immediately stored in liquid nitrogen. Specimens were baked in a laboratory furnace and moist air environment, at a temperature of 190°C (± 2°C) unless stated otherwise and over the range from 1 minute to 500 h. For uncoated specimens, exposure time was normalized by a characteristic time ($\tau = L^2/D_H$, where L is the half of sample thickness) to account for thickness variation. Cadmium plate was stripped by immersion in 300g/L NH_4NO_3 for 2 minutes.[42] Experiments indicated that this procedure did not introduce detectable levels of hydrogen into specimens that would bias the results presented here.

Determination of diffusible hydrogen concentration

The Barnacle Electrode method was used to measure diffusible hydrogen concentration, $C_{H,Diff,}$ from charged and plated samples.[43] The flat cell consisted of a hydrogen-containing specimen as the working electrode (anode), a platinized-niobium mesh as counter electrode, and a Hg/Hg_2SO_4 reference electrode. Saturated $Ca(OH)_2$ solution (pH ~ 12.1) was used as the H extraction solution in the Barnacle cell. One hour prior to and during extraction, $Ca(OH)_2$ solution was deaerated continuously using N_2. During measurement, an extraction potential of –1.00 V (*vs.* Hg/Hg_2SO_4) (330 mV anodic to E_{H/H^+}) was maintained potentiostatically. Temperature was maintained at room temperature. Diffusible H concentrations were calculated using the formula:[43]

$$C_{H\,Diff} = \frac{J_t}{zF}\left[\frac{D_H}{\pi t}\right]^{-1/2} \quad (1)$$

where J_t is the H oxidation current density recorded at time t, z is the number of electrons involved in the oxidation (1 equivalent/mol), and F is the Faraday constant (96,500 coulombs/equivalent). Eq. 1 assumes $C_{H,Diff} = 0$ at the steel surface where H is oxidized at $t > 0$ and a uniform $C_{H,Diff}$ in the steel sample at $t = 0$. Equation 1 is the first-term approximation of a complex expression and requires that $L^2/D_H t_{max} \geq 4$, where L is thickness.[43] The t_{max} is the time up to which $C_{H,Diff}$ may be calculated from the experimental value of J_t using the first term solution shown in Eq. 1. This condition was ensured for all experiments. $C_{H,Diff}$ was determined using Eq. 1 applied to the H oxidation current density at t = 300, 600 and 1200 s. Conversion to weight parts per million was done by multiplying the experimental results from Eq. 1 (as mol H/cm^3) by 1.27×10^5 based on the density of Fe-13Co-11Ni-3Cr-1Mo-0.2C steel. Hydrogen diffusion is concentration dependent and the specific H diffusivities used in Eq. 1 for each H charging overpotential were determined from prior work.[44]

Determination of fracture toughness

Compact tension (CT) specimens were machined in the C-R orientation with a width (W) of 38.1 mm and thickness (B) of 2.8 mm. Specimens were heat-treated, ground to a 600-grit surface finish and fatigue precracked using decreasing maximum stress intensity from 24.5 MPa√m to 10 MPa√m at a final crack length-to-width of

0.50. Fatigue precracking was performed on a closed loop servohydraulic test machine operated in load control at a frequency of 10 Hz. After precracking, each specimen was H charged for 20 days in 60ºC saturated $Ca(OH)_2$ at an overpotential of –0.30 V in order to achieve a 4.6 wppm diffusible H concentration.[22] One of the H-charged specimens was baked at 190°C for 24 h according to the QQ-P-416F Standard to eliminate dissolved H. Each H-charged CT specimen was stressed under rising-crack mouth opening displacement, δ, to determine the plane strain threshold stress intensity for initiation of subcritical H induced cracking at room temperature. Testing was done with a closed-loop servoelectric tensile loading machine operated under δ-feedback control with a $dK/dt=3.33 \times 10^{-2}$ MPa√m/s for as-charged specimens and 4.85×10^{-2} MPa√m/s for charged and baked specimens. Crack mouth opening displacement was measured using a clip gauge mounted across the notch mouth. Crack length was monitored continuously with the direct current potential difference technique. Load was plotted *vs.* δ for data analysis.

Determination of trap states and H occupancy by thermal desorption spectroscopy

Thermal Desorption Spectroscopy (TDS) was used to characterize H desorption and detrapping during heating processes. A detailed description of TDS is provided by Smith and Scully.[45] For cadmium plated specimens, the plated layer was stripped. Specimens were then cleaned in methanol, rinsed with distilled water, and stored in LN_2 prior to TDS tests. After background subtraction, the corrected P_{H2} - t data were transformed to data sets of H-concentration (C_H) and its rate of variation (dC_H/dt, or desorption rate) versus time or temperature (T). Specimens were tested under a temperature programmed ramp mode to characterize the H in defined trap states by locating the temperature for the desorption maximum for each trap state (i.e. peaks on dC_H/dt *vs.* T curves) and comparing with those observed for as-charged samples. Unambiguous peak identification in the case of overlapping peaks was enabled using PeakFit™ [(2)] software. A H desorption energy, E_d, was calculated using TDS data obtained at different heating rates. The peak desorption temperature, T_m, increases with heating rate, dT/dt as demonstrated for both TDS[46] and differential thermal analysis.[47] The E_d depends on T_m and dT/dt according to:[47]

$$\frac{d\left[\ln\left(\frac{dT/dt}{T_m^2}\right)\right]}{d\left[\frac{1}{T_m}\right]} = -\frac{E_d}{R} \qquad (2)$$

E_d was calculated from linear regression slope of $\ln[(dT/dt)/T_m^2]$ *vs* $1/T_m$ data, obtained from desorption maximum as a function of dT/dt. This analysis was applied to each peak observed during a temperature programmed TDS experiment. The E_d values provide the basis for estimating the binding energy, E_b, for H trapping in each of the observed states, provided that the relationship between E_d and E_b is known. In this paper E_d is assumed to equal $E_m + E_b$, where E_m is the activation energy for H diffusion by an interstitial jump mechanism in the trap-free steel lattice containing the alloy elements in the solid solution.

RESULTS

Effect of predissolved H on K_{TH} in Fe-13Co-11Ni-3Cr-1Mo-0.2C steel

Predissolved H degrades the subcritical crack growth resistance of Fe-13Co-11Ni-3Cr-1Mo-0.2C steel and the amount of degradation increases dramatically with increasing H content. The results of slow-rising δ ($dK/dt = 2.2 \times 10^{-4}$ MPa√m/s) experiments in Fig. 1 show the threshold stress intensity for the onset of stable-

[(2)] PeakFit is a product of AISN Software Inc., Mapleton, OR 97453

subcritical crack growth (K_{TH}) as a function of diffusible dissolved-H concentration.[15] The K_{TH} decreased strongly, from K_{JIC} of 132-143 MPa√m with essentially no dissolved-mobile H, to a K_{TH} less than 30 MPa√m for $C_{H,Diff}$ between 0 and 1 wppm. The level of K_{TH} decreased to less than 15 MPa√m as $C_{H,Diff}$ increased to 7.6 wppm. Testing with replicate specimens containing $C_{H,Diff}$ = of 0, 0.5, 3.9 to 4.0, 5.9, and 7.6 wppm confirmed experimental reproducibility. The dissolved H in steel caused a microscopic fracture mode transition that correlated with decreasing K_{TH}.[15] Fracture in H-free steel at high K_{JIC} occurred by microvoid coalescence (MVC). In contrast the reduction in crack growth resistance due to a $C_{H,Diff}$ of 4.6 wppm correlated with a completely brittle transgranular crack path, as shown in Fig. 2. The brittle TG character of the crack in steel intensified with increasing hydrogen content, correlating with decreasing K_{TH}.

Effect of post-H-charging baking on K_{TH} in Fe-13Co-11Ni-3Cr-1Mo-0.2C steel

Figure 3 shows load *vs.* δ data for Fe-13Co-11Ni-3Cr-1Mo-0.2C steel CT specimens that were tested after either H-precharging only or H-precharging then baking. The H charged specimen ($C_{H,Diff}$ = 4.6 wppm) exhibited severe hydrogen embrittlement as expected given the measured K_{TH} of 15.9 MPa√m. Baking the identically precharged specimen at 190ºC for 24 h eliminated all diffusible H from bare steel without a cadmium plate, as verified by electrochemical extraction (Barnacle Electrode) and TDS experiments, as discussed in an ensuing section. Hydrogen elimination correlated with a complete reversal in IHE and restored fracture resistance to K_{JIC} = 123 MPa√m, which essentially equals the fracture resistance of as-received Fe-13Co-11Ni-3Cr-1Mo-0.2C steel without precharged H. An SEM image of the fracture surface of the H-charged and baked specimen revealed that the brittle TG fracture mode was restored to MVC typical of this steel with $C_{H,Diff}$ = 0 wppm, Fig. 4.

Hydrogen trapping states in Fe-13Co-11Ni-3Cr-1Mo-0.2C steel

Fig. 5 shows representative H desorption results (dC_H/dt versus temperature) measured during temperature-programmed TDS. For the temperature range from 23 to 500ºC, at least three desorption peaks are identified and marked as peak 1b, 2 and 3 in the order of increasing peak temperature T_m. For low temperatures preceding peak 1b, a "shoulder" exists on the dC_H/dt versus temperature curve; this peak was particularly apparent for heating at the higher dT/dt values. The analysis procedure described above and Eq. 2 were used to determine E_d for trap state 1b. This analysis is shown in Fig. 6. Table 4 lists the E_b values determined for H in the four unique trap states in Fe-13Co-11Ni-3Cr-1Mo-0.2C steel, charged to two different albeit similar diffusible H concentrations and using a lattice-migration energy of E_m = 10 kJ/mol.[36]

To clarify the connection between $(Fe,Cr,Mo)_2C$ precipitates and the trap states shown in Fig. 5, temperature-programmed TDS tests were performed for specimens with the as-quenched microstructure heated at various dT/dt.[36] The area for peak 1b in the as-quenched alloy was substantially decreased compared with aged alloy, and a new small peak (1a) was apparent in the vicinity of peak 1b but at a temperature higher than the shoulder observed for the aged steel. TDS tests at other dT/dt produced similar results. Based on the area under the dC_H/dt *vs.* time curve, the amount of H, desorbed over the temperature range where peak 1b appeared for the aged alloy, decreased by 98% for the as-quenched case.[36] The amount of H desorption associated with peak 1a for the as-quenched alloy was only ~2% of that of peak 1b seen only in the aged alloy. The as-quenched martensitic microstructure does not contain $(Fe,Cr,Mo)_2C$ precipitates that are predominant in the aged alloy.[5] This proves that the coherent $(Fe,Cr,Mo)_2C$ precipitates in the aged martensite alloy are the trapping sites responsible for formation of the dominant peak 1b. This trap state is reversible, characterized by an E_b of 11.4 – 11.6 kJ/mol, and represented by an incredibly high ratio of trap sites to lattice sites of 0.03 – 0.07.[36] The $(Fe,Cr,Mo)_2C$ in peak hardened alloy maintains considerable coherency with the matrix, as suggested by strains inferred from contrast patterns in transmission electron microscopy images.[48] This coherent interface explains the low E_b associated with peak 1b, as binding energy decreases with increasing interface coherency.[49] Quantitative analysis yielded identical-high E_b values for peaks 2 and 3 in the as-quenched and aged forms of Fe-13Co-11Ni-3Cr-1Mo-0.2C steel. The strong trap state with E_b of 61.3-62.2 kJ/mol is likely associated with martensite interfaces, austenite grain boundaries, and mixed dislocation cores. Undissolved metal carbides and highly misoriented grain boundaries likely trap H with the highest binding energy determined (E_b = 89.1-89.9 kJ/mol). The microstructural features that cause peaks 2 and 3 do not change during tempering.

Residual trapped hydrogen in charged and baked uncoated Fe-13Co-11Ni-3Cr-1Mo-0.2C steel

Concerning precharged steel without a coating, the amount of H egressed increases significantly with increasing time at the baking temperature, and the amount of residual hydrogen decreases continually, as shown in Figs. 7 and 8. The diffusible hydrogen concentration measured by the Barnacle Electrode method (Fig. 7) decreases at all baking times. Diffusible hydrogen was essentially removed after $t/\tau \geq 1$. Regarding TDS data (Fig. 8), there is an obvious decrease in the height and area coverage of the dC_H/dt *vs.* T curves, particularly for peak 1b after each baking time at 190°C. The "shoulder" associated with peak 1 disappears after 5 minutes of baking. Within 30 minutes, peak 1b on desorption rate curve disappears as a result of substantial H egress. Based on trap state identification, this suggests that hydrogen trapped at $(Fe,Cr,Mo)_2C$ carbides is removed after sufficient baking time at 190°C.[36] However, hydrogen trapped at peaks 2 and 3 remains.[(3)]

For each peak in Fig. 8, the H concentration was calculated by integrating the dC_H/dt versus time curve for the range of time corresponding to the peak coverage. Fig. 9 shows the variation of H concentration for baked specimens, $C_{H(baked)}$, relative to that of the as-charged specimen, $C_{H(as\text{-}charged)}$, expressed as percentage for each peak. For the shoulder, there was a dramatic change in the relative H concentration in the initial 5 minutes of baking ($t/\tau \leq 0.6$). $C_{H(baked)}/C_{H(as\text{-}charged)}$ dropped to ~20% after baking for $t/\tau = 0.12$ and to near zero after baking for $t/\tau = 0.6$. Concerning peak 1b, the change was less dramatic. $C_{H(baked)}/C_{H(as\text{-}charged)}$ was reduced to ~60% after baking for $t/\tau = 0.12$. Peak 1b was eliminated after baking for $t/\tau = 3.6$. For peaks 2 and 3, $C_{H(baked)}/C_{H(as\text{-}charged)}$ increased to more than 160% after baking for $t/\tau = 0.12$. Following this increase, $C_{H(baked)}/C_{H(as\text{-}charged)}$ decreased for both peak 2 and 3 but was never eliminated after baking for t/τ at least up to 3.6. This decrease was not definitive because of the relatively low levels of dC_H/dt and the variability associated with the data recorded from these peaks.

All diffusible hydrogen (measured by the Barnacle Electrode method), as well as the H trapped at $(Fe,Cr,Mo)_2C$ carbides associated with peak 1b, is readily removed by baking at 190°C given a sufficient and relatively short baking time. The detrapping of such H corresponded with complete restoration of fracture toughness and the corresponding ductile fracture mode (Figs. 3 and 4). Therefore, removal of H from trap state 1b is crucial to recovery of fracture toughness. It is technologically important to determine whether such detrapping can be achieved in Cd-plated and baked Fe-13Co-11Ni-3Cr-1Mo-0.2C steel after baking at the same temperature.

Residual trapped and diffusible hydrogen in cadmium plated and baked Fe-13Co-11Ni-3Cr-1Mo-0.2C steel

The coating thickness and porosity of two different batches of dull-Cd plated Fe-13Co-11Ni-3Cr-1Mo-0.2C steel are indicated in Figs. 10-13. The thicknesses of these layers of Cd are 18 μm and 10 μm, and the thin layer appears to be more porous. This is a qualitative judgment since porosity was not quantified. Figure 14 illustrates the change in residual diffusible hydrogen concentration after baking with a thick Cd layer. The relative diffusible hydrogen concentration first increases with baking time, reflecting additional H entry into the steel from the Cd layer that contains codeposited hydrogen. At very long baking times relative to uncoated and H-precharged steel (Fig. 7), the diffusible hydrogen concentration is lowered. This process is hindered by the Cd layer, which serves as a permeation barrier,[13] and the slow H diffusivity in Fe-13Co-11Ni-3Cr-1Mo-0.2C steel.[22,44] Diffusible H content data are not available for the thin, more porous cadmium plate shown in Figs. 12 and 13.

TDS data are shown in Figs. 15 and 16 for the thin and thick Cd coatings, respectively. In addition to trap states 1b, 2 and 3, an additional unidentified state is also seen. This peak 1a is uncovered due to the low overall hydrogen content of the Cd-plated specimens relative to the specimens precharged in $Ca(OH)_2$ solution, especially the absence of the large shoulder adjacent to peak 1b in Fig. 5. There are distinct differences between the TDS data taken after various baking times for thin *vs.* thick cadmium plated steel. For the thin coating, the residual hydrogen associated with peak 1a decreases at short baking times, while that associated with state 1b first rises

(3) Note that dC_H/dt is plotted logarithmically in Fig. 5, but on a linear axis in Fig. 8; only the former clearly reflects the H egress that constitutes peaks 2 and 3.

then decreases as a function of time (Fig. 17). However, over 100 h of baking are required to reduce the residual hydrogen associated with peak 1b. Concerning the thicker Cd layer, both peaks 1a and 1b increase as a function of baking time (Fig. 18). After long baking times, residual H associated with peak 1a is eliminated. However, the status of H associated with peak 1b is unclear, but it does not appear to have been reduced significantly. For both thin and thick Cd layers, H associated with trap states 2 and 3 may be decreased, but only by a modest percentage, and this conclusion is confounded by low peak heights and measurement variability. Based on these results, short baking times could promote IHE, and very long baking times are required to remove damaging-diffusible H, even for the thin-porous Cd plated layer and certainly for thick Cd with low porosity.

DISCUSSION

Correlation between detrapping of hydrogen and restoration of fracture toughness

All diffusible hydrogen (Barnacle Electrode measurements) as well as H trapped at $(Fe,Cr,Mo)_2C$ carbides (peak 1b) is removed by baking at 190°C in both uncoated and porous-cadmium coated Fe-13Co-11Ni-3Cr-1Mo-0.2C steel given sufficient baking time. The detrapping of such hydrogen corresponded with complete restoration of fracture toughness and transition from a brittle TG to ductile MVC fracture mode (Fig. 3 and 4). Trap state 1b has a binding energy of 11.4-11.6 kJ/mol and a desorption energy of 21.4-21.6 kJ/mol. The results of these TDS experiments demonstrate that 190°C baking readily removes the detrimental hydrogen from $(Fe,Cr,Mo)_2C$ traps, as expected theoretically because the thermal energy of baking at 190°C is similar to this trap binding energy and overall trap desorption energy so as to enable a high probability of hydrogen release from trap sites (e.g., kT_{190C}= 3.85 kJ/mol ≈ 11.5±0.5 kJ/mol). However, H egress is unfortunately retarded by both the slow H diffusivity in this steel[15,22] and by the cadmium plated coating that functions as a permeation barrier.[13] Specifically, thick and thin cadmium plated coatings both intensify the H levels retained in the steel upon short to intermediate term 190°C baking, up to about 50 h, as seen in Figs. 15-18. Longer term baking removes hydrogen associated with interstitial lattice sites and unidentified weaker traps (peak 1a), as well as at $(Fe,Cr,Mo)_2C$ trap sites (peak 1b), when cadmium plated coatings are thin and porous as shown in Figs. 15 and 17. However, thicker cadmium coatings with lower porosity are a more permanent barrier to H egress. In this case, hydrogen associated with $(Fe,Cr,Mo)_2C$ traps (peak 1b) is not removed by long term baking at 190°C, as seen in Figs. 16 and 18. The absolute values of these times are correct for the Cd-plated thin specimens that were characterized, but are not directly relevant to plated components. Rather, the time for H egress must be determined by a diffusion analysis that includes the Cd barrier thickness, H content, and H diffusivity, as well as geometry of the UHSS component in question.

These results suggest that H may be retained in trap state 1b, the finely dispersed strengthening precipitates, when dull cadmium layers are thick and less porous. Such residual trapped hydrogen is thus available to affect the fracture resistance of Fe-13Co-11Ni-3Cr-1Mo-0.2C steel, at least near the surface of thick sections even after long baking times. In contrast, hydrogen associated with trap states 2 and 3 was not removed by 190°C baking in bare or Cd plated steel. These hydrogen trap states do not govern subcritical H-enhanced cracking, but may alter fracture toughness at faster loading rates that is governed by microvoid fracture.[15] It is worth reviewing the fundamental reason why the removal of hydrogen associated with trap state 1b, in particular, is crucial to control and mitigation of time-dependent subcritical IHE in this UHSS.

The role of traps in time-dependent subcritical IHE

IHE in high strength alloys can be exacerbated by a high density of sites for reversible trapping of H, as well as stronger trapping at sites that constitute a connected crack path through the microstructure. Such behavior is demonstrated by the low threshold stress intensity (K_{TH}) for transgranular IHE in peak aged Fe-13Co-11Ni-3Cr-1Mo-0.2C steel containing bulk-dissolved diffusible H concentration in excess of 0.5 to 10 wppm.[15] This behavior was explained by the hypothesis that, upon stressing, H repartitions from low to moderate strength reversible trap sites and is attracted to the crack tip stress field in an amount that depends on the relative values of E_b and the stress field-H interaction energy. TEM observations show that the $(Fe,Cr,Mo)_2C$ spacing is 20–50 nm.[5,48] The plastic zone size for the threshold of IHE in Fe-13Co-11Ni-3Cr-1Mo-0.2C steel is of order 50 μm at

K = 30 MPa√m and contains a substantial amount of $(Fe,Cr,Mo)_2C$ trap sites as the H source. This H is attracted to process zone traps with higher binding energies in the range of 30-60 kJ/mol and interconnected to yield a TG crack path. Such features could include interfaces associated with the martensitic microstructure and vacancy clusters from H-deformation interaction.[30] Identification of the high density of $(Fe,Cr,Mo)_2C$ sites for reversible trapping of H in this steel, as well as the four H-trap binding energies summarized in Table 4 further establish this explanation.

From thermodynamic consideration, lattice H concentration is enhanced from an unstressed lattice-soluble level of C_L to a stress-affected $C_{H\sigma}$ depending on the magnitude of the crack tip hydrostatic stress, σ_H:[50]

$$C_{H\sigma} = C_L \, exp\left(\frac{\sigma_H V_H}{RT}\right) \tag{3}$$

assuming dilute H concentration, negligible effect of dissolved H on elastic constants of the material, and no negative deviation from the logarithmic proportionality between $C_{H\sigma}$ and σ_H.[51,52] The H concentration at trap sites in the crack tip process zone is related to the local lattice H solubility, provided that local equilibrium exists, and is thus enhanced by dilatational stress to $C_{H\sigma T}$, according to:[24]

$$C_{H\sigma T} = C_{H\sigma} \, exp\left(\frac{E_b}{RT}\right) = C_L \, exp\left(\frac{E_b + \sigma_H V_H}{RT}\right) \tag{4}$$

Hydrogen repartitions from a reversible trap state to the crack tip if the stress field interaction energy, $\sigma_H V_H$, exceeds the $E_{b\text{-Source}}$ for the supplying trap near the tensile hydrostatic stress field, following Eq. 4. The amount of accumulated crack tip H is governed by the sum of $\sigma_H V_H$ and $E_{b\text{-Fracture Sites}}$, where this binding energy is for the highest energy trap state in the stress field and that provides the interconnected crack path.

The results in Fig. 19 establish that the $(Fe,Cr,Mo)_2C$ trap state is a likely H-supply source to enable low K_{TH} for IHE in Fe-13Co-11Ni-3Cr-1Mo-0.2C steel. The three measured E_b for this steel are shown by the horizontal-dashed lines, with the lowest energy state (11.4 to 11.6 kJ/mol in Table 4) corresponding to $(Fe,Cr,Mo)_2C$ interface traps and the intermediate energy (61.3-62.2 kJ/mol in Table 4) for disordered interfaces including martensite packet and lath surfaces. The binding energy for H trapped at vacancies and vacancy clusters is between 40 and 70 kJ/mol,[30] also well above E_b for trapping at $(Fe,Cr,Mo)_2C$. The plotted values (Δ) of crack tip interaction energy are given by $\sigma_H V_H$. However, the crack tip stress state is controversial for low stress intensity cracking typical of IHE, and to account for this uncertainty, the ordinate covers a range of hydrostatic stress levels normalized to the tensile yield strength of Fe-13Co-11Ni-3Cr-1Mo-0.2C steel.[9] Classical continuum fracture mechanics suggests that σ_H is 2.5 σ_{YS} for a low strain hardening UHSS.[53,54] Analysis based on either a crack tip dislocation perspective,[24,55,56] or strain gradient plasticity hardening included in the flow curve,[57,58] suggest that σ_H may be as high as $8\sigma_{YS}$. The former lower stress estimate of interaction energy (9 kJ/mol) is less than the $(Fe,Cr,Mo)_2C$ binding energy of 11.5 kJ/mol, while the high stress estimate corresponds to higher interaction energy of 27 kJ/mol in Fig. 19.

The extent of H repartition from reversible $(Fe,Cr,Mo)_2C$ traps to the crack tip is given by:[59,60]

$$P_\sigma = \frac{exp\left[\sigma_H V_H \big/ RT\right]}{exp\left[\sigma_H V_H \big/ RT\right] + exp\left[E_b \big/ RT\right]} \tag{5}$$

where P_σ is the probability given in infinite time that H occupies a lattice site in the fracture process zone under the influence of the crack tip hydrostatic stress field *vs.* occupation of trap sites near the crack tip at $(Fe,Cr,Mo)_2C$ interfaces. With the measured E_b of 11.5 kJ/mol, this probability is 0.22 for the low estimate of σ_H ($2.5\sigma_{YS}$) and 0.998 for the higher bound of $8\sigma_{YS}$. For each case, and particularly for the higher crack tip stresses, there is a significant probability for H repartition from this dominant low energy trap state to the crack tip.

This source of internal H from $(Fe,Cr,Mo)_2C$ traps, as well as the high level of $C_{H\sigma T}$ that can accumulate at martensite interfaces in the crack tip process zone (10^{14} C_L from Eq. 4, assuming that $\sigma_H = 5\ \sigma_{YS}$, and exceeding 100 wt pct assuming that C_L is of order 10^{-4} wppm), explain the severe IHE produced in precharged steel at low $K_{TH} \sim 0.1\ K_{IC}$ in the absence of baking.[15] Notably, this hydrogen embrittlement was eliminated by baking the H-charged specimen at 190°C for 24 h, which effectively removed H from the low temperature shoulder and trap state 1b [$(Fe,Cr,Mo)_2C$ interfaces] based on TDS characterization of the H charged and baked microstructure.[61] Heating at 190°C did not eliminate H from trap states 2 and 3. However, this strongly trapped H did not produce embrittlement since the comparison in Fig. 19 shows that the probability for H repartition to the crack tip is very low when residual H is only present in traps with $E_b \sim 60$ kJ/mol; from Eq. 5, P_σ is 10^{-6} even for $\sigma_H = 8\ \sigma_{YS}$. However, such strongly trapped residual H may enhance microvoid fracture. This potential problem has not been investigated.

Control of IHE by microstructural manipulation

Analysis of the energetics of H partitioning in a FPZ suggests a metallurgical approach to improve the IHE resistance of aged Fe-13Co-11Ni-3Cr-1Mo-0.2C steel. The coherence of $(Fe,Cr,Mo)_2C$ decreases and Cr/Mo clusters are eliminated by aging at temperatures above about 500°C.[5] The resulting precipitates should have higher H-binding energies than 11.5 kJ/mol, typical of incoherent interfaces, and alloy yield strength will be reduced modestly. These changes will tend to reduce H repartitioning from the reversible trap sites at $(Fe,Cr,Mo)_2C$ to the crack tip hydrostatic tensile stress field, as illustrated by the argument summarized in Fig. 19. If the reduction is sufficiently large and if aging does not introduce another reversible trap state, then H damage will be reduced.[15] Experiments are required to test this speculation and establish the balance between the tensile strength, fracture toughness and IHE resistance of Fe-13Co-11Ni-3Cr-1Mo-0.2C steel. A similar approach could be based on reductions in $(Fe,Cr,Mo)_2C$ coherence by alloying element addition.[62]

Either approach to reducing TG hydrogen embrittlement could augment the important–prior development of IG hydrogen cracking resistance derived from reduced metalloid segregation through impurity control to produce IHE resistant UHSS.[9] This broad development would represent a breakthrough in high performance structural materials. Since H supply is uniquely different for IHE and HEE, understanding of the interaction of crack tip trap sites and H must be extended to the hydrogen environment case where the damaging H is delivered to FPZ damage sites from the electrochemically active crack tip surface and over a sub-micrometer distance.[63] This H transport situation is fundamentally different from that which governs IHE in UHSS.

Control of IHE in cadmium plated Fe-13Co-11Ni-3Cr-1Mo-0.2C steel

We have established the technical basis for controlling IHE through understanding of hydrogen-microstructure interactions that play a strong role in IHE, with emphasis on crack tip process zone damage. This is a more scientific approach than the established methodology based on trial and error analysis of the effects of various thermal baking treatments on fracture toughness of plated steels. The results presented here provide a scientific understanding of which hydrogen trap states exist in Fe-13Co-11Ni-3Cr-1Mo-0.2C steel, and which control internal hydrogen embrittlement. If this information is coupled with knowledge of the trap states that release hydrogen for egress during remedial baking procedures, then strategies for controlling IHE emerge. Control of IHE in cadmium plated UHSS such as Fe-13Co-11Ni-3Cr-1Mo-0.2C steel requires that the following considerations be adhered to; Note that these comments only apply to IHE with a finite quantity of internal hydrogen.

1. The damaging source of hydrogen during IHE is from those trap sites as well as interstitial lattice sites that are the source for repartitioning of H to the tensile stress field of a crack tip where it retraps. By definition, these damaging traps that supply hydrogen must have low enough binding energies such that $E_b < \sigma_H v_H$. Therefore, thermal baking must be performed to remove diffusible hydrogen from such trap states that energetically allow hydrogen repartitioning to the crack tip fracture process zone. In the case of Fe-13Co-11Ni-3Cr-1Mo-0.2C steel, this requires that the thermal energy imparted by baking approaches the desorption energy (e.g., $kT_{baking} \approx E_d = E_m + E_b$) of $(Fe,Cr,Mo)_2C$ traps or others that supply damaging hydrogen to the crack tip. This concept also requires that thermal energy imparted during baking approach the desorption energy of diffusible H from the crack tip stress field in an UHSS; that is $kT_{baking} \approx \sigma_H v_H + E_m$. If this is the case, then H will be eliminated from reversible trap sites that can supply embrittling H during IHE as summarized in Fig. 19.
2. Sufficiently long baking times are required to avoid short term intensification of hydrogen levels in cadmium-plated ultra-high strength steels including Fe-13Co-11Ni-3Cr-1Mo-0.2C steel. This phenomenon results from hydrogen ingress supplied from electrochemically co-deposited H existing in cadmium layers. This occurs during early baking periods at 190°C.
3. Control of dull cadmium plated layer thickness and porosity is necessary so that thermal egress of hydrogen from weak trap states such as $(Fe,Cr,Mo)_2C$ precipitates in Fe-13Co-11Ni-3Cr-1Mo-0.2C steel is not hindered by the H-barrier action of the coating.
4. Microstructural control of trapping states must be optimized such that strong traps, that do not release hydrogen upon 190°C baking, cannot themselves serve as crack initiation sites or be interconnected to provide a continuous crack propagation path. Trap states 2 and 3 in Fe-13Co-11Ni-3Cr-1Mo-0.2C steel do not form such a propagation paths, but may affect microvoid fracture.

Moreover, microstructural control is necessary to avoid a high density of intermediate binding energy trap states that resist thermal egress of hydrogen (e.g., $kT_{baking} << E_d$), but allow repartitioning of hydrogen to the stress field of extremely sharp crack tips (e.g., $E_b < \sigma_H v_H$) with associated high hydrostatic stress levels. It appears fortuitous that $(Fe,Cr,Mo)_2C$ traps do not fall into this category and instead satisfy the criteria listed in (1) above. However, this is not assured for all ultra-high strength steels in all applications under all H producing conditions, including IHE and HEE.

CONCLUSIONS

(1) Fe-13Co-11Ni-3Cr-1Mo-0.2C steel, processed for ultra-high strength and fracture toughness, exhibits at least three distinct hydrogen trap states in a complex precipitation hardened martensitic microstructure and is susceptible to severe internal hydrogen embrittlement (IHE) at threshold stress intensity levels as low as 20 MPa$\sqrt{m}$.

(2) The causes of IHE susceptibility include very high crack-tip tensile stresses and a reservoir of diffusible hydrogen that is trapped reversibly with a binding energy, E_b, of 11.5±0.5 kJ/mol at $(Fe,Cr,Mo)_2C$ precipitates. This reversibly trapped hydrogen repartitions to interstitial sites proximate to the highly stressed crack tip and, subsequently, may retrap at martensitic lath interfaces to produce substantial local hydrogen concentrations and transgranular embrittlement.

(3) 190°C baking readily removes the detrimental diffusible hydrogen associated with $(Fe,Cr,Mo)_2C$ traps and other low energy sites in electrochemically precharged but unplated Fe-13Co-11Ni-3Cr-1Mo-0.2C steel. Such hydrogen detrapping and egress correlates directly with a restoration in ultra-high fracture toughness and a ductile fracture mode. Hydrogen trapped at higher trap binding energy sites is not removed by 190°C baking, but cannot redistribute to the crack tip fracture process zone and does not participate in subcritical hydrogen cracking.

(4) 190°C baking eventually removes the detrimental hydrogen associated with $(Fe,Cr,Mo)_2C$ traps in cadmium-plated steel as long as the cadmium-plated layer is thin and porous. However, the internal H

concentration in Fe-13Co-11Ni-3Cr-1Mo-0.2C steel at such traps is at first intensified upon baking of cadmium-plated steel for short time periods as a consequence of H supply from as-deposited cadmium-plated layers. H egress occurs at long baking times but is retarded by the slow H diffusivity in steel and the barrier action of the cadmium plating.

ACKNOWLEDGEMENTS

Financial support from the Office of Naval Research, Grant Number N00014-91-J-4164 with Dr. A. John Sedriks as the Scientific Officer, is gratefully acknowledged. Current support under Grant Number N00014-03-1-0029 with Dr. Airan Perez is also gratefully actnowledged. Princeton Applied Research and Scribner Associates, Inc. support electrochemical instrumentation in the Center for Electrochemical Science and Engineering at the University of Virginia.

REFERENCES

1. M.G.H. Wells, *Key Engineering Materials*, Vol. 77-78, pp. 71-80, 1993.
2. G.B. Olson, *Advanced Materials and Processes*, pp. 72-9, July 1997.
3. R.M. Hemphill and D.E. Wert, *U. S. Patent Number 5,087,415,* Carpenter Technology Corporation, Reading, PA, February 11, 1992.
4. W.M. Garrison Jr., *Journal of Metals*, Vol. 46, pp. 20-4, 1990.
5. R. Ayer and P.M. Machmeier, *Metallurgical Transactions A*, Vol. 24A, pp. 1943-55, 1993.
6. C.H. Yoo, H.M. Lee, J.W. Chan and J.W. Morris, *Metallurgical and Materials Transactions A,* Vol. 27A, pp. 3466-72, 1996.
7. C.J. Kuehmann, *Thermal Processing Optimization of Nickel-Cobalt Ultrahigh-Strength Steels*, Ph.D. Dissertation, Northwestern University, Evanston, IL, 1994.
8. G.B. Olson, in *Innovations in Ultra-High Strength Steel Technology, 34th Sagamore Army Materials Conference*, US Army Laboratory Command, Watertown, MA, pp. 3-65, 1987.
9. R.P. Gangloff, in *Comprehensive Structural Integrity*, I. Milne, R.O. Ritchie and B. Karihaloo, editors-in-Chief, Vol. 6, Elsevier Science, New York, NY, pp. 31-101, 2003.
10. E.U. Lee, H. Sanders, and B. Sarkar, *Proc. Tri-Service Conf. On Corrosio*n, J.V. Kelley and B. Placzankis, editors, Army Research Laboratory, Aberdeen, MD, CD file S08p2a.pdf, 2000.
11. P. Buckley, B. Placzankis, J. Beatty, and R. Brown, *Corrosio*n/*9*4, paper no. 547, NACE, Houston, TX, 1994.
12. P.F. Buckley, R. Brown, G.H. Graves, E.U. Lee, C.E. Neu, and J. Kozol, in *Metallic Materials for Lightweight Applications, 40th Sagamore Army Materials Research Conf*., M.G.H. Wells, E.B. Kula, and J.H. Beatty, editors, United States Army Laboratory Command, Watertown, MA, pp. 377-88, 1993.
13. J.B. Boody and V.S. Agarwala, *Corrosion /87*, paper no. 224, NACE, Houston, TX, 1987.
14. D.A. Berman, *Materials Performance*, Vol. 24, pp. 36-41, 1985.
15. R.L.S. Thomas, J.R. Scully, and R.P. Gangloff, *Metallurgical and Materials Transactions A,* Vol. 34A, pp. 327-44, 2003.
16. G.N. Vigilante, J.H. Underwood, and D. Crayton, in *Fatigue and Fracture Mechanics, Proc. 30th Nat. Symp*., ASTM STP 1360, ASTM International, West Conshohocken, PA, pp. 377-87, 2000.
17. E.U. Lee: *Metallurgical Transactions* A, Vol. 26A, pp. 1313-6, 1995.

18. H.E.Townsend, *Corrosion*, Vol. 37, no. 2, pp. 115-20, 1981.

19. B850-98: Standard Guide for Post-Coating Treatment of Steel for Reducing Risk of Hydrogen Embrittlement, *Annual Book of ASTM Standards Vol. 02.05*, ASTM International, West Conshohocken, PA, pp. 613-5, 2001.

20. M.J. Robinson and R.M. Sharp, *Corrosion*, Vol. 41, no. 10, pp. 582-86, 1985.

21. T. Zhong-Zhuo, H. Chi-Mei, L. Rong-Bong, F. Yi-Feng, and C. Xiang-Rong, in *Current Solutions to Hydrogen Problems in Steels*, C.G. Interrante and G.M. Pressouyre, editors, ASM International, Materials Park, OH, p. 98-103, 1982.

22. R.L.S. Thomas, *Internal Hydrogen Embrittlement of a Trap-Rich Ultra-High Strength Steel AerMet® 100*, MS Thesis, University of Virginia, Charlottesville, VA, 2000.

23. E.L. Williams and D.M. Anderson, *Materials Performance*, Vol. 24, no. 12, pp. 9-12, 1985.

24. W.W. Gerberich, T. Livne, X.-F. Chen, and M. Kaczorowski, *Metallurgical Transactions A*, Vol. 19A, pp. 1319-34, 1988.

25. G.M. Pressouyre and F.M. Faure, in *Hydrogen Embrittlement: Prevention and Control, ASTM STP 962*, L. Raymond, editor, ASTM, Philadelphia, PA, pp. 353-71, 1988.

26. G.M. Pressouyre and I.M. Bernstein, *Metallurgical Transactions A*, Vol. 9A, pp. 1571-80, 1978.

27. G.M. Pressouyre, in *Hydrogen Effects in Metals*, I.M. Bernstein and A.W. Thompson, editors, The Minerals, Metals, and Materials Society, Warrendale, PA, pp. 27-36, 1981.

28. K.Yamakawa, S. Yonezawa and S. Yoshizawa, in *International Congress on Metallic Corrosion*, National Research Council, Toronto, Canada, pp. 254-61, 1984.

29. R.P. Gangloff, in *Corrosion Prevention and Control*, M. Levy and S. Isserow, editors, U.S. Army Materials Technology Laboratory, Watertown, MA, pp. 64-111, 1986.

30. M. Nagumo, M. Nakamura and K. Takai, *Metallurgical and Materials Transactions A*, Vol. 32A, pp. 339-47, 2001.

31. G.M. Pressouyre and I.M. Bernstein, *Acta Metallurgica*, Vol. 27, pp. 89-100, 1979.

32. M.F. Stevens and I.M. Bernstein, *Metallurgical Transactions A*, Vol. 16A, pp. 1879-86, 1985.

33. J.R. Scully, J.A. Van Den Avyle, M.J. Cieslak, A.D. Romig and C.R. Hills, *Metallurgical Transactions A*, Vol. 22A, pp. 2429-43, 1991.

34. G.M. Pressouyre, *Acta Metallurgica,* Vol. 28, pp. 895-911, 1980.

35. N. Suzuki, N. Ishii and T. Miyagawa, *Tetsu-to-Hagane* (*Journal of the Iron and Steel Institute of Japan*), Vol. 82, no. 2, pp. 170-5, 1996.

36. D. Li, R.P. Gangloff and J.R. Scully, "Hydrogen Trap States in Ultrahigh-Strength AerMet® 100 Steel", submitted to *Metallurgical and Materials Transactions A,* in press, 2003.

37. *Alloy Data-AerMet® 100 Alloy*, Carpenter Technology Corporation Carpenter Steel Division, Reading, PA, 1992.

38. J.M. Dahl, "Ferrous-Base Aerospace Alloys"*, Advanced Materials and Processes*, pp. 33-6, 2000.

39. J.F. Shackelford, *Introduction to Materials Science for Engineers,* Fifth Edition, Prentice Hall, Upper Saddle River, New Jersey, pp. 164-8, 2000.

40. QQ-P-416F, *Plating, Cadmium (Electrodeposited),* Federal Specification, Naval Air Engineering Center, Systems Emgineering and standardization Department, Lakehurst, NJ April 1986.

41. B487-85 *Standard Test Method for Measurement of Metal and Oxide Coating Thickness by Microscopical Examination of a Cross Section,* Annual Book of ASTM Standards, Vol. 02.05, ASTM, Philadelphia, PA, pp. 237-240, 1991.

42. B767-88 *Standard Guide for Determining Mass Per Unit Area of Electrodeposited and Related Coatings by Gravimetric and Other Chemical Analysis Procedures,* Annual Book of ASTM Standards, Vol. 02.05, ASTM, Philadelphia, PA, pp. 555-560, 1991.

43. J.J. DeLucia and D.A. Berman, *An Elecrochemical Tecnique to Measure Diffusible Hydrogen in Metals (Barnacle Electrode),* In Electrochemical Corrosion Testing, ASTM STP 727, F. Mansfeld and U. Bertocci, editors, ASTM, Philadelphia, PA, pp. 256-273, 1981.

44. R.L.S. Thomas, D. Li, R.P. Gangloff and J.R. Scully, *Metallurgical and Materials Transactions - A*, Vol. 33A, pp. 1991-2003, 2002.

45. S.W. Smith and J.R. Scully, *Metallurgical and Materials Transactions-A,* Vol. 31A, pp. 179-93, 2000.

46. J.Y. Lee, J.L. Lee and W.Y. Choo, *Current Solutions to Hydrogen Problems in Steels*, ASM, Metals Park, OH, pp. 423-7, 1982.

47. H.E. Kissinger, *Analytical Chemistry*, Vol.29, pp. 1702-6, 1957.

48. R. Ayer and P.M. Machmeier, *Metallurgical and Materials Transactions A*, Vol. 29A, p. 903-5, 1998.

49. D.L. Johnson, G. Krauss, J.K. Wu and K.P. Tang, *Metallurgical Transactions A*, Vol. 18A, pp. 717-21, 1987.

50. R.A. Oriani, in *Fundamental Aspects of Stress Corrosion Cracking*, NACE, Houston, TX, pp. 32-50, 1969.

51. J.P. Hirth, *Metallurgical Transactions A*, Vol. 11A, pp. 861-90, 1980.

52. W.C. Johnson and J.Y. Huh, "Thermodynamics of Stress-induced Interstitial Redistribution in BCC Metals", *Metallurgical and Materials Transactions A*, in press, 2003.

53. K.N. Akhurst and T.J. Baker, *Metall. Trans.* A, Vol. 12A, pp. 1059-70, 1981.

54. T.L. Anderson, *Fracture Mechanics: Fundamentals and Applications,* 2nd Ed., CRC Press, Boca Raton, FL, pp. 117-81, 1995.

55. Y. Katz, N. Tymiak and W.W. Gerberich, *Engineering Fracture Mechanics*, Vol. 68, pp.619-46, 2001.

56. X. Chen and W.W. Gerberich, *Metallurgical Transactions A,* Vol. 22A, pp. 59-70, 1991.

57. Y. Wei and J.W. Hutchinson, *Journal of Mechanics and Physics of Solid*s, Vol. 45, pp. 1253-73, 1997.

58. H. Jiang, Y. Huang, Z. Zhuang and K.C. Hwang, *Journal of Mechanics and Physics of Solid*s, Vol. 49, pp. 979-93, 2001.

59. T.Y. Zhang and J.E. Hack: *Metallurgical and Materials Transactions A,* Vol. 30A, pp. 155-9, 1999.

60. T.Y. Zhang, H. Sheu and J.E. Hack, *Scripta Metallurgica et Materialia*, Vol. 27, pp. 1605-1610, 1992.

61. D. Li, R.P. Gangloff and J.R. Scully, *Hydrogen Diffusion and Trapping Behavior in Ultrahigh Strength AerMet® 100 Steel*, Technical Report, University of Virginia, Charlottesville, VA, 2002.

62. R. Ayer and P.M. Machmeier, *Metallurgical Transactions*, 27A, pp.2510-21, 1996.

63. R.P. Gangloff, in *Hydrogen Effects on Material Behavior and Corrosion Deformation Interactions*, N.R. Moody, A.W. Thompson, R.E. Ricker, G.S. Was and R.H. Jones, eds., The Minerals, Metals & Materials Society, Warrendale, PA, pp. E03:1-21, 2003.

TABLE 1
EXAMPLES OF CURRENT BAKING PRACTICE FOR SOME HIGH STRENGTH STEELS

Steel Type	Temperature (^{o}C)	Time (h)	Reference
Tensile strength of 1201-1800 MPa	190-220	min. 12 - 22	[19]
Engineering Cr-plated items	440-480	min. 1	[19]
Surface-hardened parts	130-160	min. 8-16	[19]
Cd-coated parts	190	5 - 24	[13]
AISI 1080	191	3	[18]
Cd-coated AISI 4340 and 300M	190	>100	[14]
High carbon steel	200	2	[20]

TABLE 2
CHEMICAL COMPOSITION OF Fe-13Co-11Ni-3Cr-1Mo-0.2C STEEL (wt%) [15]

Fe	Co	Ni	Cr	Mo	C	P	S	H (wppm)
Bal.	13.40	11.10	3.10	1.20	0.23	0.003	0.0008	0.35

TABLE 3
MECHANICAL PROPERTIES OF HEAT-TREATED Fe-13Co-11Ni-3Cr-1Mo-0.2C STEEL [15, 37]

Orientation	Yield Strength		Ultimate Tensile Strength		Elongation	Charpy V-Notch Impact Energy		Fracture Toughness K_{IC}	
	Ksi	MPa	Ksi	MPa	%	Ft-lbs	J	Ksi√in	MPa√m
L	250	1724	285	1965	14	30	41	115	126
T	250	1724	285	1965	13	25	34	100	110

L: Longitudinal, T: Transverse

TABLE 4
CALCULATED VALUES OF TRAP BINDING ENERGIES, E_b, kJ/mol (eV/atom) IN Fe-13Co-11Ni-3Cr-1Mo-0.2C STEEL USING E_m = 10 kJ/mol [36]

η_{chg}	Peak 1a *	Peak 1b **	Peak 2	Peak 3
-0.62V	8.9±0.2 (0.092±0.002)	11.6±0.2 (0.120±0.002)	62.2±0.3 (0.644±0.003)	89.1±0.3 (0.924±0.003)
-1.17V	-------	11.4±0.2 (0.118±0.002)	61.3±0.3 (0.635±0.003)	89.9±0.3 (0.932±0.003)

* for as-quenched alloy ** for aged alloy

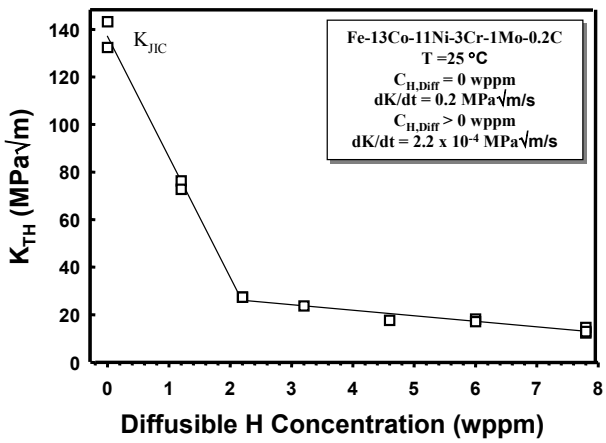

FIGURE 1. Threshold stress intensity for hydrogen embrittlement, K_{TH}, of Fe-13Co-11Ni-3Cr-1Mo-0.2C steel at various diffusible H concentrations obtained during pre-charging.[15]

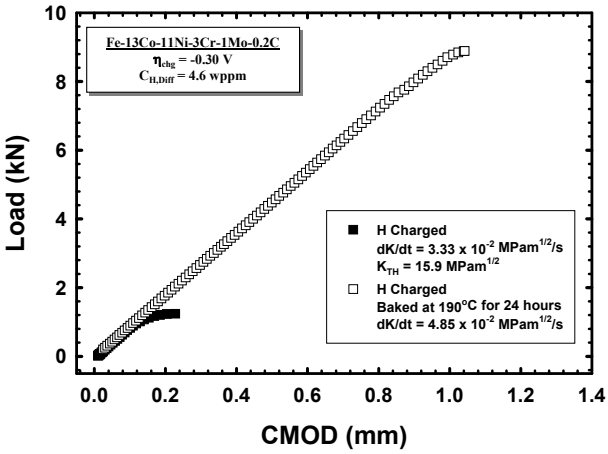

FIGURE 3. Load versus CMOD data for H precharged ($C_{H,Diff}$ = 4.6 wppm) and precharged/baked Fe-13Co-11Ni-3Cr-1Mo-0.2C steel. Charging was conducted in saturated $Ca(OH)_2$ at overpotential of –0.30 V at 60ºC for 20 days. Baking was performed at 190 °C for 24 hours.[15]

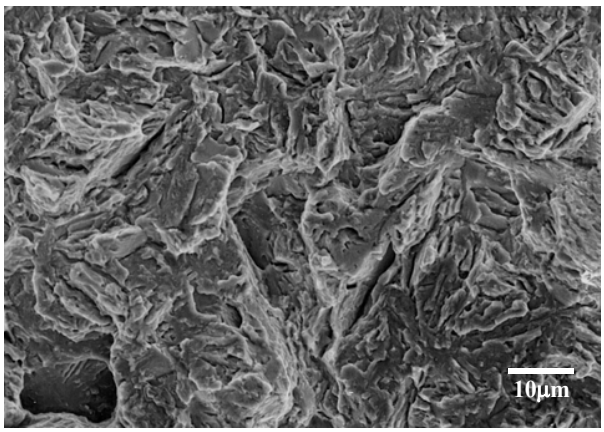

FIGURE 2. Scanning electron image of the fracture surface of Fe-13Co-11Ni-3Cr-1Mo-0.2C steel with diffusible H concentration of 4.6 wppm. Fracture occurred completely by a brittle transgranular mode. Crack growth was from top to bottom.[15]

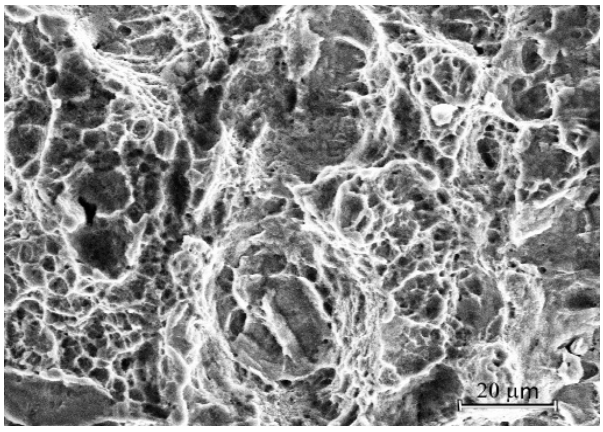

FIGURE 4. Scanning electron image of the fracture surface of hydrogen-charged Fe-13Co-11Ni-3Cr-1Mo-0.2C steel after baking at 190 °C for 24 hours. The specimen was previously charged to a diffusible H concentration of 4.6 wppm.

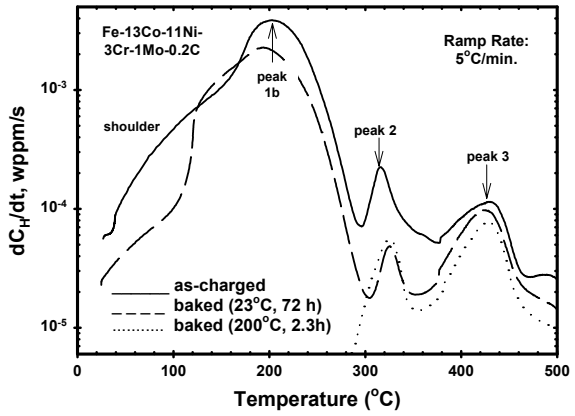

FIGURE 5. H desorption rate as a function of temperature for peakaged Fe-13Co-11Ni-3Cr-1Mo-0.2C steel, measured by TDS at a ramp heating rate of 5°C/min, showing the effect of baking compared with the as-charged condition (charged at overpotential of –0.62 V at 60°C).[36]

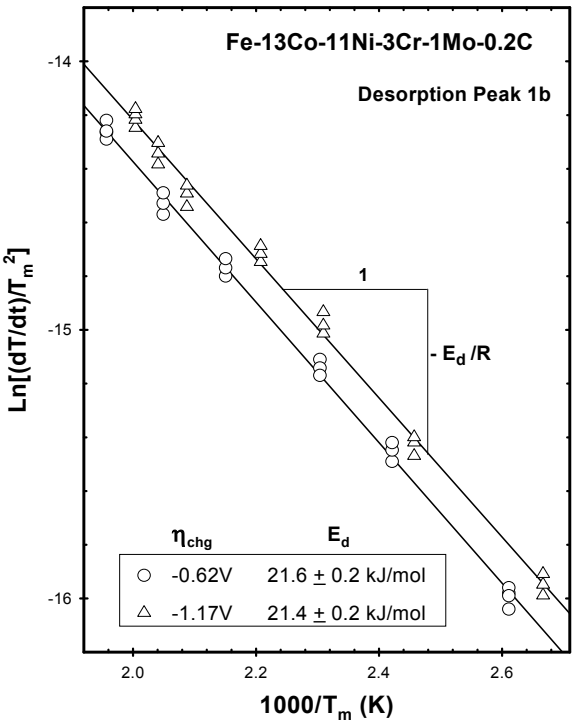

FIGURE 6. Experimental determination of the apparent activation energy for H desorption, E_d, associated with detrapping-peak 1b from the H desorption curves for peakaged Fe-13Co-11Ni-3Cr-1Mo-0.2C steel.[36]

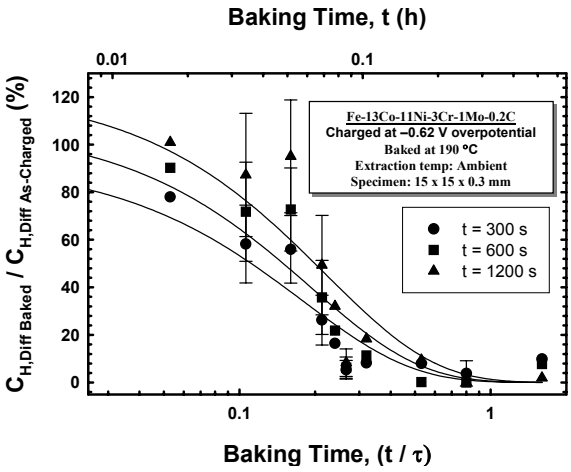

FIGURE 7. Residual diffusible H concentrations in hydrogen charged and baked peakaged Fe-13Co-11Ni-3Cr-1Mo-0.2C steel (without cadmium coating) after the indicated baking times expressed as t/τ ($\tau = L^2/D$, L = 0.015 cm and $D_{eff} = 2 \times 10^{-7}$ cm^2/sec). Results are shown for the various times (t) used to calculate $C_{H,Diff}$ values from Equation 1 and are normalized to as-charged values. Measurements were performed using the Barnacle Electrode method and background was subtracted. (Standard deviation given, when three or more tests were conducted)

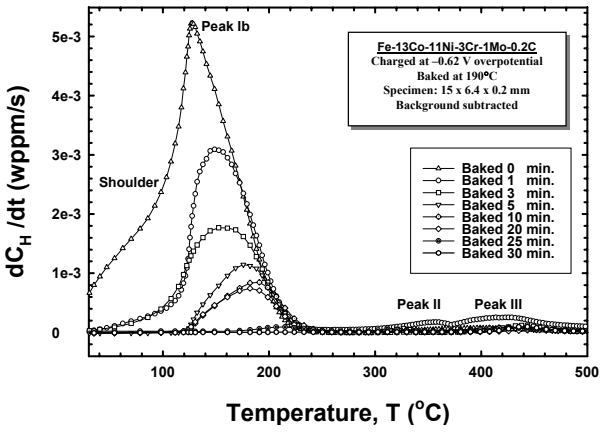

FIGURE 8. Hydrogen desorption rates versus TDS ramp temperature for H precharged and baked uncoated Fe-13Co-11Ni-3Cr-1Mo-0.2C steel specimens after the indicated baking times at 190 °C. TDS tested at dT/dt = 5 °C. Charging was performed in saturated $Ca(OH)_2$.

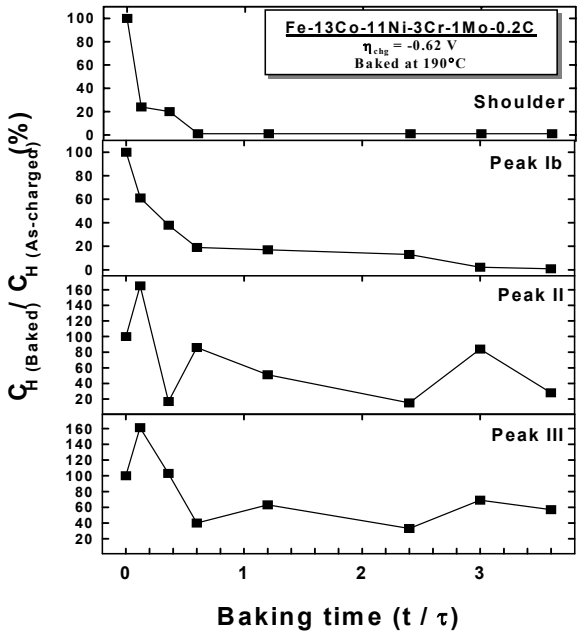

FIGURE 9. Percentage of the H concentration egressed from each peak of $Ca(OH)_2$ precharged and baked uncoated Fe-13Co-11Ni-3Cr-1Mo-0.2C steel specimens, $C_{H\ Baked}$, relative to the corresponding concentration for the as-charged specimen, $C_{H\ As\text{-}charged}$. Results were reported versus t/τ where t is baking time (sec.) and τ is the time constant ($\tau = L^2/D$, L = 0.01 cm and $D_{eff} = 2 \times 10^{-7}$ cm^2/sec).

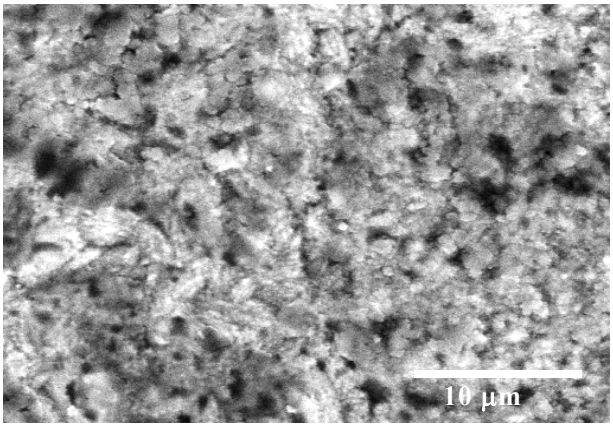

FIGURE 10. SEM micrograph of the as-plated surface of a thick cadmium deposit on Fe-13Co-11Ni-3Cr-1Mo-0.2C steel.

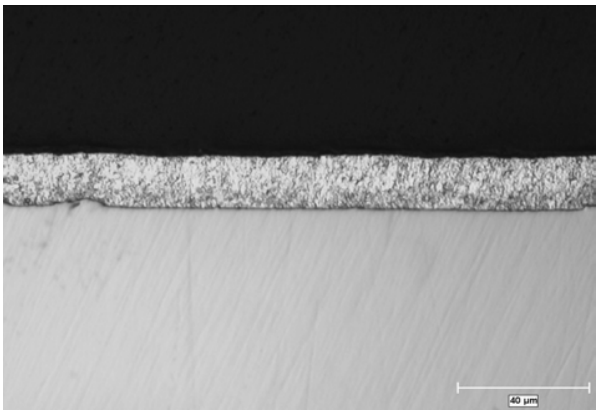

FIGURE 11. Cross section of thick cadmium plated Fe-13Co-11Ni-3Cr-1Mo-0.2C steel examined using optical microscopy.

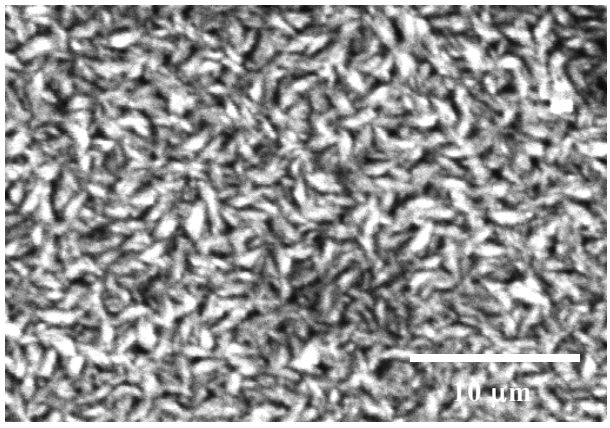

FIGURE 12. SEM micrograph of the as-plated surface of a thin cadmium deposit on Fe-13Co-11Ni-3Cr-1Mo-0.2C steel.

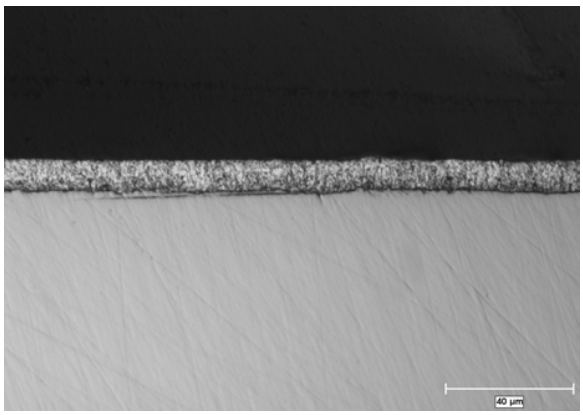

FIGURE 13. Cross section of thin cadmium plated Fe-13Co-11Ni-3Cr-1Mo-0.2C steel examined using optical microscopy at 400X magnification.

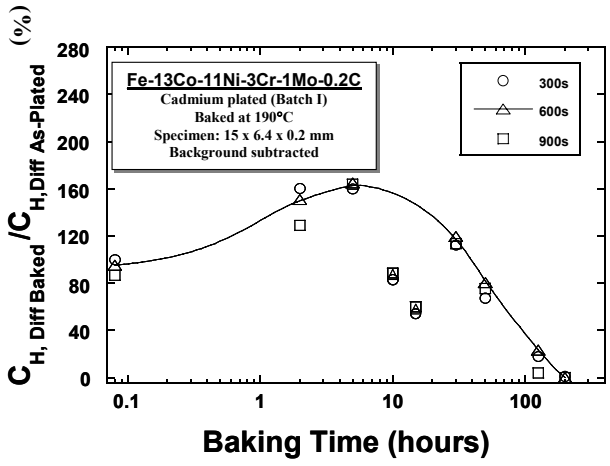

FIGURE 14. Residual diffusible H concentration from thick cadmium plated Fe-13Co-11Ni-3Cr-1Mo-0.2C steel after the indicated baking time. Concentrations were calculated for three different t values, where t is the extraction time used in Equation 1. Results are normalized to the as-plated value.

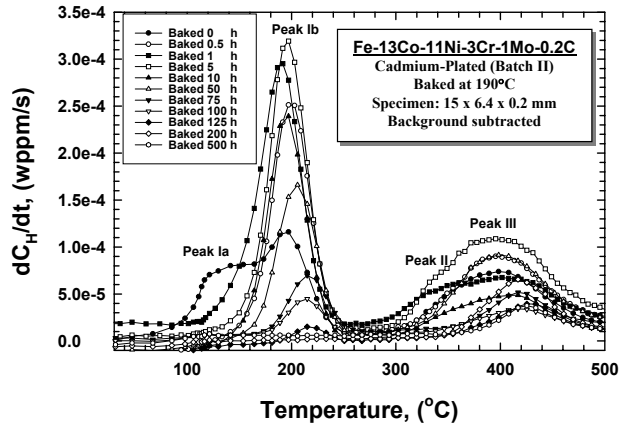

FIGURE 15. Hydrogen desorption rate versus TDS ramp temperature for thin cadmium plated and baked Fe-13Co-11Ni-3Cr-1Mo-0.2C steel specimens after the indicated baking time at 190 °C. TDS tested at dT/dt = 5 °C.

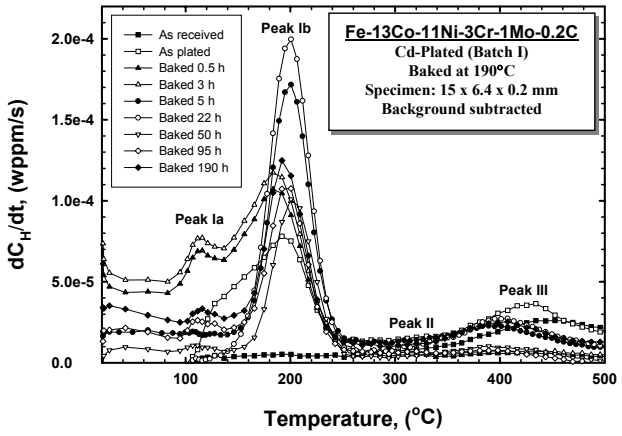

FIGURE 16. Hydrogen desorption rate versus TDS ramp temperature for thick cadmium plated and baked Fe-13Co-11Ni-3Cr-1Mo-0.2C steel specimens after the indicated baking time at 190 °C. TDS tested at dT/dt = 5 °C.

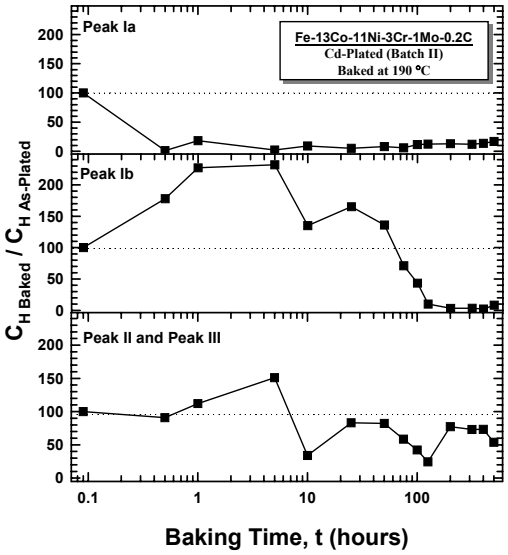

FIGURE 17. Residual H concentration associated with each peak identified from the H desorption curves of thin cadmium plated and baked Fe-13Co-11Ni-3Cr-1Mo-0.2C steel specimens as a function of baking time. Results are normalized to the as-plated value and expressed as % of initial H concentration. Background was subtracted. Coating thickness ~ 10 μm.

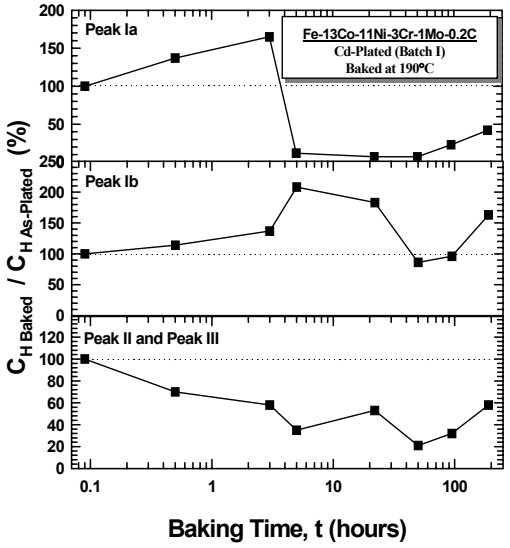

FIGURE 18. Residual H concentration associated with each peak identified from the H desorption curves of thick cadmium plated and baked Fe-13Co-11Ni-3Cr-1Mo-0.2C steel specimens expressed as a function of baking time. Results are normalized to the as-plated values and expressed as % of initial H concentration. Background was subtracted. Coating thickness ~ 18 μm.

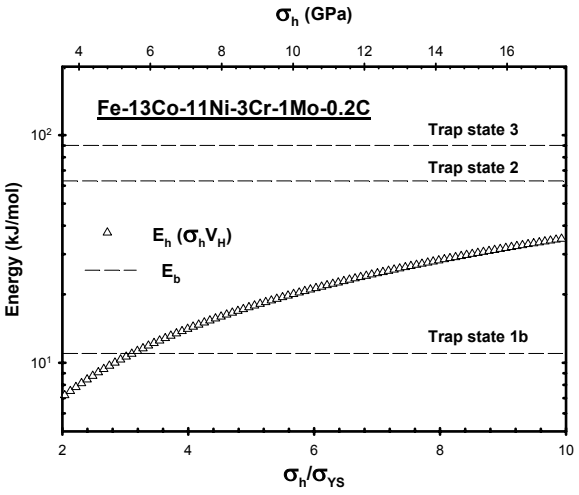

FIGURE 19. The interaction energy E_h (= $\sigma_h V_H$) associated with a given hydrostatic tensile stress, σ_h, ahead of the crack tip compared with E_b for major trap states in aged Fe-13Co-11Ni-3Cr-1Mo-0.2C steel, where V_H, the partial molar volume of H in Fe, is 2.0 cm^3/mol.